Temporal and tissue-specific activation of AHR signaling in discrete models of kidney disease

AHR Reporter Mouse Model

B6.Cg-Tg(DRE-lacZ)2Gswz/J

Induction of Renal Injury

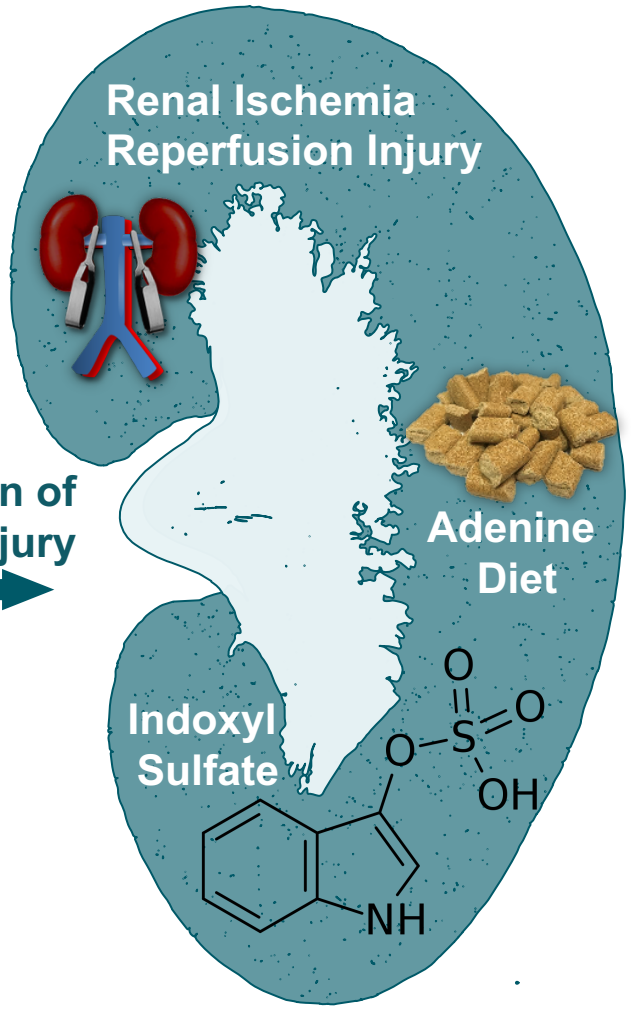

Assessment of AHR Activation

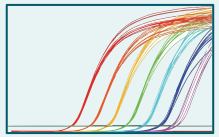
qRT PCR

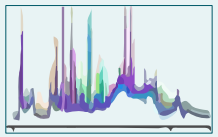
Metabolomics

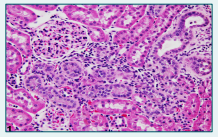
Histology

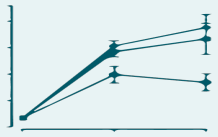
Renal Function

Results

Increased AHR activation

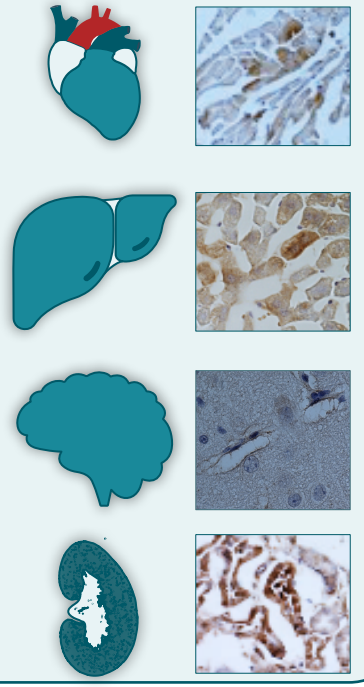

CONCLUSION:

Specific tissues in several organs demonstrated the AHR activation in response to uremia.

These results may explain some of the systemic manifestations of indolic solute toxicity.

KI REPORTS
KIReports.org

Walker, 2019

Temporal and tissue-specific activation of aryl hydrocarbon receptor in discrete mouse models of kidney disease

Joshua A. Walker[1,2], Sean Richards[1], Mostafa E. Belghasem[3], Nkiruka Arinze[1], Sung Bok Yoo[1], Joseph Y. Tashjian[1], Stephen A. Whelan[4], Norman Lee[4], Vijaya B. Kolachalama[2], Jean Francis[1], Katya Ravid[2], David Sherr[5] and Vipul C. Chitalia[1,6,7]

[1]Renal Section, Department of Medicine, Boston University School of Medicine, Boston, Massachusetts, USA; [2]Whitaker Cardiovascular Institute, Boston University, Boston, Massachusetts, USA; [3]Department of Pathology and Laboratory Medicine, Boston University School of Medicine, Boston, Massachusetts, USA; [4]Department of Chemistry, Boston University, Boston, Massachusetts, USA; [5]Department of Environmental Health, Boston University School of Medicine, Boston, Massachusetts, USA; [6]Veteran Affairs Boston Healthcare System, Boston, Massachusetts, USA; and [7]Global Co-Creation Labs, Institute of Medical Engineering and Science, Massachusetts Institute of Technology, Cambridge, Massachusetts, USA

Emerging evidence in animal models of chronic kidney disease (CKD) implicates Aryl Hydrocarbon Receptor (AHR) signaling as a mediator of uremic toxicity. However, details about its tissue-specific and time-dependent activation in response to various renal pathologies remain poorly defined. Here, a comprehensive analysis of AHR induction was conducted in response to discrete models of kidney diseases using a transgenic mouse line expressing the AHR responsive-promoter tethered to a β-galactosidase reporter gene. Following validation using a canonical AHR ligand (a dioxin derivative), the transgenic mice were subjected to adenine-induced and ischemia/reperfusion-induced injury models representing CKD and acute kidney injury (AKI), respectively, in humans. Indoxyl sulfate was artificially increased in mice through the drinking water and by inhibiting its excretion into the urine. Adenine-fed mice showed a distinct and significant increase in β-galactosidase in the proximal and distal renal tubules, cardiac myocytes, hepatocytes, and microvasculature in the cerebral cortex. The pattern of β-galactosidase increase coincided with the changes in serum indoxyl sulfate levels. Machine-learning–based image quantification revealed positive correlations between indoxyl sulfate levels and β-galactosidase expression in various tissues. This pattern of β-galactosidase expression was recapitulated in the indoxyl sulfate–specific model. The ischemia/reperfusion injury model showed increase in β-galactosidase in renal tubules that persisted despite reduction in serum indoxyl sulfate and blood urea nitrogen levels. Thus, our results demonstrate a relationship between AHR activation in various tissues of mice with CKD or AKI and the levels of indoxyl sulfate. This study demonstrates the use of a reporter gene mouse to probe tissue-specific manifestations of uremia in translationally relevant animal models and provide hypothesis-generating insights into the mechanism of uremic toxicity that warrant further investigation.

Correspondence: *Vipul C. Chitalia, Department of Medicine, Boston University Medical Center, Evans Biomedical Research Center, X-530, Boston, Massachusetts 02118, USA. E-mail: vichital@bu.edu*

Received 21 December 2018; revised 17 September 2019; accepted 26 September 2019; published online 30 October 2019

Kidney International (2020) **97,** 538–550; https://doi.org/10.1016/j.kint.2019.09.029

KEYWORDS: acute kidney injury; aryl hydrocarbon; chronic kidney disease; uremia

Published by Elsevier, Inc., on behalf of the International Society of Nephrology.

Translational Statement

Uremic solutes contribute to the pathogenesis of some of the systemic complications in patients with chronic kidney disease. Among different solutes, tryptophan metabolites such as indolic solutes are the ligands of the aryl hydrocarbon receptor, a ubiquitously expressed protein associated with several diseases. Here, using a reporter gene mouse, we show tissue-specific activation of the aryl hydrocarbon receptor in different organs in models of chronic kidney disease and acute kidney injury. Clinically, this work provides hypothesis-generating insights into the manifestations of uremia and strengthens the potential exploration of aryl hydrocarbon receptor inhibitors to reduce the organ level toxicity of uremic solutes in patients with chronic kidney disease.

Chronic kidney disease (CKD) is a progressive disease resulting from irreversible alterations in kidney structure and function. Approximately 10% of the adult population in the United States and worldwide suffer from CKD, and the incidence of, and mortality due to, CKD is increasing.[1] CKD is characterized by the retention of a heterogeneous mix of metabolites, collectively referred to as *uremic solutes*. They are retained early in the blood of patients with CKD and persist even after hemodialysis.[2,3] The systemic complications associated with CKD (grouped as uremic manifestations) are in part driven by these compounds.[4,5]

Of these uremic toxins, indolic solutes (such as indoxyl sulfate [IS]) are particularly pathogenic and have protean manifestations in the vascular system, such as inducing oxidative stress and suppressing fundamental endothelial functions.[6,7] Our work and that of others in animal models and humans implicate indolic uremic solutes in the hyperthrombotic CKD milieu by activating tissue factor in the endothelial and vascular smooth muscle cells.[8–11] Indolic solutes have both profibrotic and proinflammatory effects on cardiac tissue[12,13] and also are linked to toxicity in microglia.[14] This evidence clearly demonstrates the multisystem effects of indolic solutes.

The aryl hydrocarbon receptor (AHR) pathway is emerging as a mediator of toxicity by indolic solutes.[8] AHR is a ligand-activated transcription factor, classically known to mediate effects of exposure to environmental toxins such as 2,3,7,8-tetrachlorodibenzodioxin (TCDD).[15] AHR is activated not only by exogenous chemicals but also by endogenous ligands, such as 6-formylindole[3,2-b]carbazole and kynurenine, and those generated by a combination of exogenous (microbiome) and endogenous (liver) metabolism such as IS.[16,17] Research by our group and others showed that indolic solutes activate the AHR pathway in cultured cells as demonstrated by its nuclear translocation and induction of cell type–specific AHR target genes and followed by degradation of the AHR protein.[8–10]

AHR has been implicated independently in diseases related to the cardiovascular system[18,19] and the central nervous system.[20] Given its activation in the uremic milieu, AHR is likely to contribute to some of the systemic manifestations of indolic uremic solutes. Despite the importance of the AHR pathway in uremic toxicity, there are no studies examining the kinetics and tissue-specific pattern of AHR activation in discrete models of renal diseases. We set out to examine these specific questions using a transgenic mouse (B6.Cg-Tg(DRE-lacZ)2Gswz/J) with a β-galactosidase reporter gene downstream of 2 AHR dioxin response elements (DREs).

RESULTS

We confirmed the hemizygous status of the B6.Cg-Tg(DRE-lacZ)2Gswz/J transgenic mouse line using genotyping (Supplementary Table S1) and the copy number of the *lacZ* transgene using quantitative real-time polymerase chain reaction (Supplementary Figure S1). Tissues from these mice subjected to adenine-induced CKD, ischemic/reperfusion (I/R)-induced acute kidney injury (AKI), and IS-specific models were examined at different time points (Figure 1).

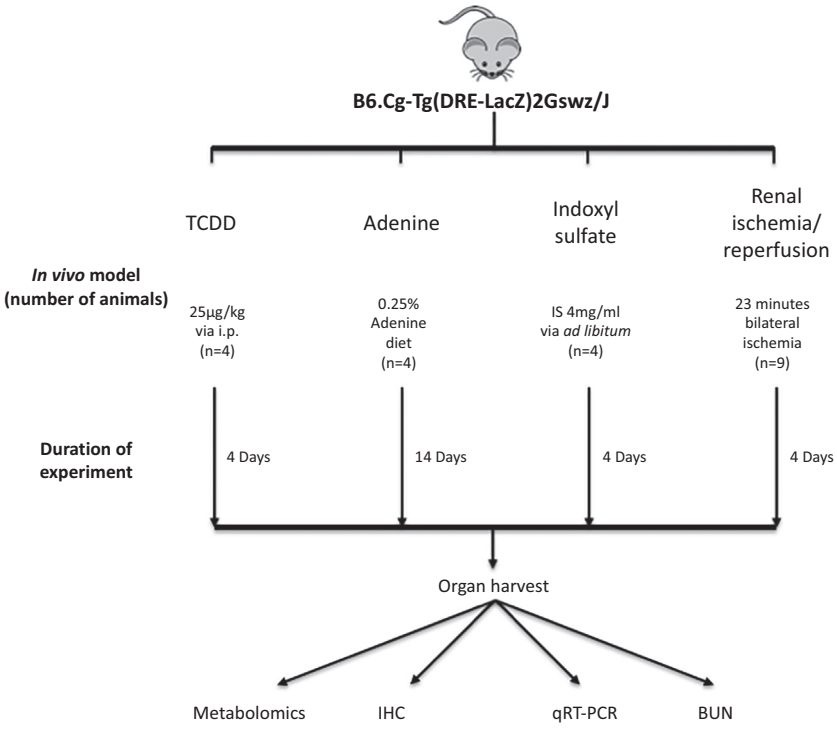

Figure 1 | Experimental design to examine aryl hydrocarbon receptor (AHR) activation in discrete models of renal disease. A combination of male and female B6.Cg-Tg(DRE-LacZ)2Gswz/J transgenic mice with an *lacZ* reporter gene downstream of 2 dioxin response elements (DREs) were subjected to 4 models. Transgenic mice treated with 2,3,7,8-tetrachlorodibenzodioxin (TCDD) (n = 4) served as a positive control. Transgenic mice (n = 4) were subjected to a 0.25% adenine–supplemented diet for 2 weeks to induce chronic kidney disease.[10] Four transgenic mice on a normal mouse diet served as controls. An indoxyl sulfate (IS)–specific model consisted of 4 transgenic mice that received IS with probenecid. Four mice exposed to probenecid alone served as controls. Renal ischemic/reperfusion was used as a model of acute kidney injury. Nine transgenic male mice were used and killed at specific time points after 23 minutes of bilateral renal ischemia and killed at 24, 48, and 96 hours postsurgery. Three additional transgenic mice served as controls after a sham surgery. BUN, blood urea nitrogen; IHC, immunohistochemistry; qRT-PCR, quantitative real-time polymerase chain reaction.

Validation of the transgenic model

Previously this transgenic mouse was used to demonstrate the teratogenic effects of the AHR pathway by exposing pregnant mothers to TCDD.[21] Although those studies provided a proof of activation of the transgene, they were performed in fetuses. Given the use of adult mice for all our disease models, we first validated this transgenic model in a group of 8- to 12-week-old mice exposed to TCDD, a potent AHR agonist. Mice treated with vehicle served as controls. Activation of the AHR pathway in TCDD-treated mice was demonstrated by a significant elevation in *β-galactosidase* mRNA from the lysates of the kidney, liver, and heart (Figure 2a). Compared with control animals, *β-galactosidase* mRNA was increased by 22.5% in the kidney ($P = 0.0481$), 26% in the liver ($P = 0.0286$), and 29.8% in the heart ($P = 0.0223$) in TCDD-treated mice. These results demonstrated induction of the AHR pathway. To detect β-galactosidase protein in different tissues, we performed both β-galactosidase enzyme assays and immunohistochemistry using prevalidated anti–β-galactosidase antibody.[22] The latter method provided a distinct and specific signal and was used for subsequent studies (Supplementary Figure S2).

TCDD-treated mice showed β-galactosidase expression in several organs (Figure 2b) including renal tubules (Figure 2b, asterisk). However, a distinct absence of β-galactosidase was noted in the glomeruli (Figure 2b, arrowhead). Liver sections of TCDD-treated animals showed a uniform β-galactosidase expression in hepatocytes, whereas patchy expression was noted in the cardiac myocytes (Figure 2b, arrowhead). AHR activation indicated by β-galactosidase expression in various tissues upon TCDD treatment validates this model.

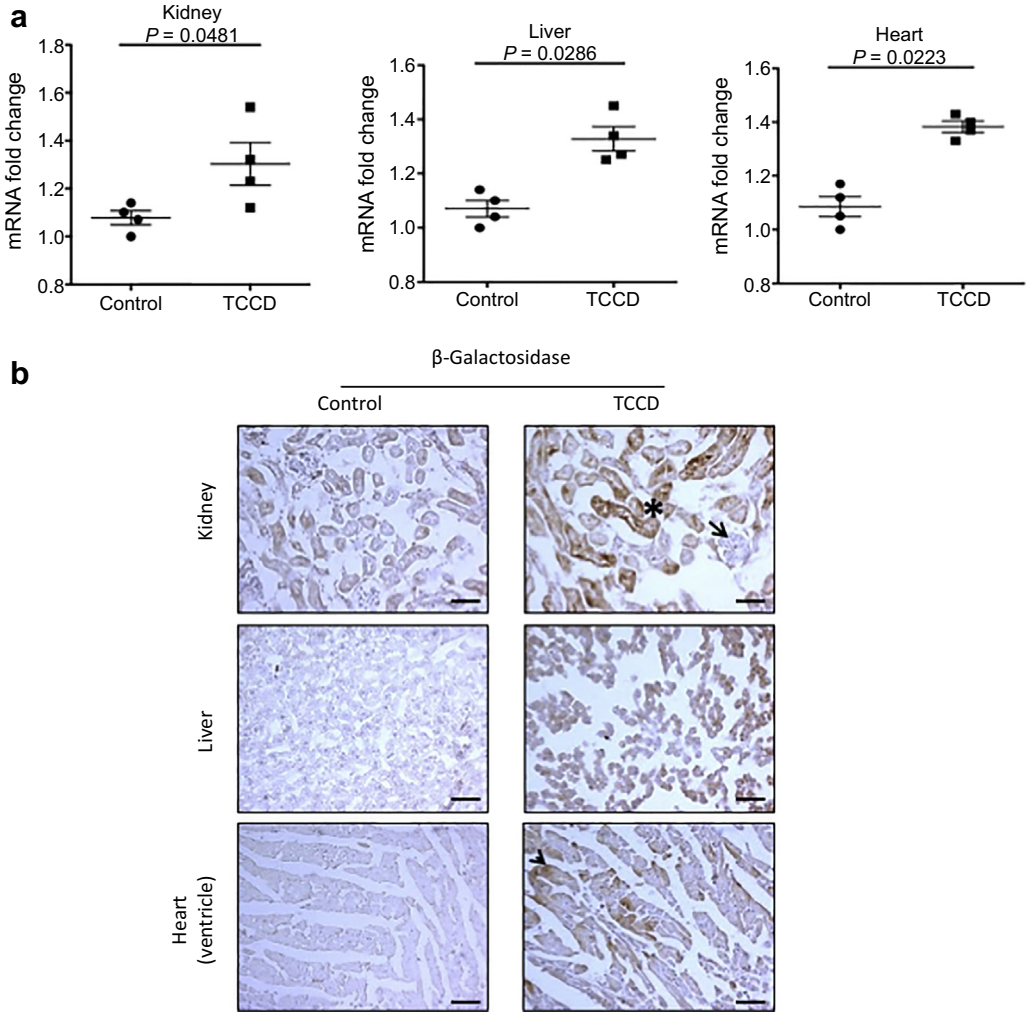

Figure 2 | Validation of transgenic mice. (**a**) β-Galactosidase mRNA was examined in whole tissue lysates from 2,3,7,8-tetrachlorodibenzodioxin (TCDD)–treated and control transgenic mice. mRNA levels were normalized to glyceraldehyde-3-phosphate dehydrogenase mRNA. Each data point represents the average of duplicate samples for each transgenic mouse used. (**b**) Frozen sections from TCDD- and control-treated transgenic animals were stained with anti–β-galactosidase antibody to examine tissue-specific expression. The β-galactosidase protein was localized to renal tubules (marked by a black asterisk) but not in glomeruli (black arrowhead), liver hepatocytes, and cardiac myocytes (black arrow). All data are expressed as mean ± SEM. Images were taken at original magnification ×200. Bar = 50 μM. To optimize viewing of this image, please see the online version of this article at www.kidney-international.org.

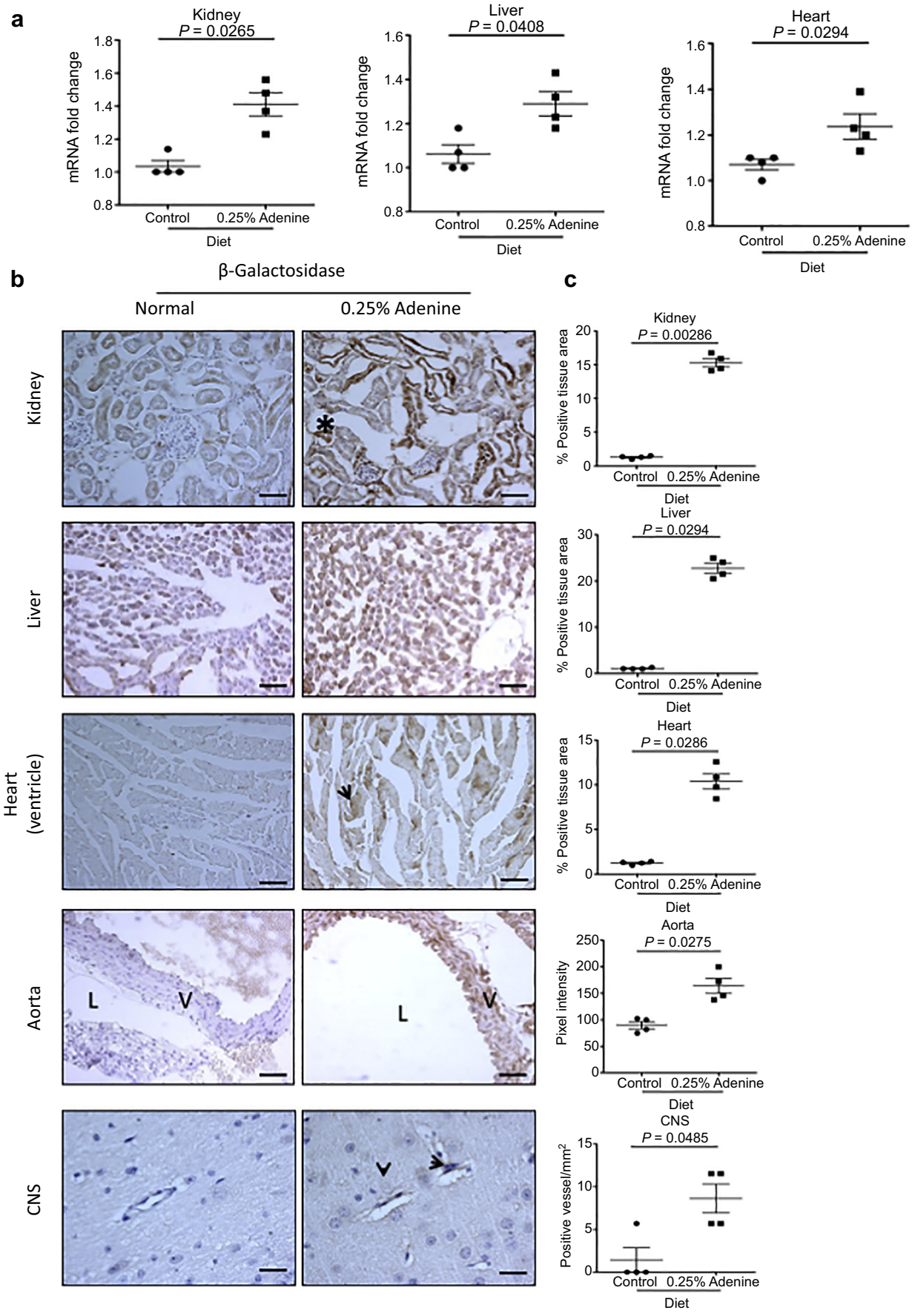
a
Kidney
P = 0.0265
mRNA fold change
1.8
1.6
1.4
1.2
1.0
0.8
Control
0.25% Adenine
Diet
Liver
P = 0.0408
mRNA fold change
1.6
1.4
1.2
1.0
0.8
Control
0.25% Adenine
Diet
Heart
P = 0.0294
mRNA fold change
1.6
1.4
1.2
1.0
0.8
Control
0.25% Adenine
Diet
b
β-Galactosidase
Normal
0.25% Adenine
Kidney
Liver
Heart (ventricle)
Aorta
CNS
L
V
c
Kidney
P = 0.00286
% Positive tissue area
20
15
10
5
0
Control
0.25% Adenine
Diet
Liver
P = 0.0294
% Positive tissue area
30
20
10
0
Control
0.25% Adenine
Diet
Heart
P = 0.0286
% Positive tissue area
15
10
5
0
Control
0.25% Adenine
Diet
Aorta
P = 0.0275
Pixel intensity
250
200
150
100
50
0
Control
0.25% Adenine
Diet
CNS
P = 0.0485
Positive vessel/mm2
15
10
5
0
Control
0.25% Adenine
Diet

AHR activation in an adenine-induced CKD model

We next examined AHR activation in an adenine-induced model, an established model of crystal-induced CKD characterized by extensive renal tubular damage and interstitial fibrosis.[10] In different animal models of CKD,[23] we used the adenine-induced CKD model because of the presence of several features of uremia in this model. Exposure to a 0.25% adenine–supplemented diet for 2 weeks in mice resulted in a significant increase in blood urea nitrogen (BUN) levels (Supplementary Figure S3A).[10] AHR activation in adenine-induced CKD mice was confirmed by a significant upregulation of *β-galactosidase* mRNA in the kidney (37.5%), liver (22.7%), and heart (16.8%) lysates (Figure 3a).

To estimate the extent of AHR activation within different tissues, a customized, color-based image segmentation pipeline was used to quantify the amount of β-galactosidase and was normalized to the tissue area (details in the Supplementary Methods and Supplementary Figure S4A).[24] Our results showed a significant increase in β-galactosidase in the kidney (10.65-fold) of adenine-treated mice, predominantly expressed in the renal tubules and the periglomerular region (Figure 3b and c, and Supplementary Figure S5, original magnification ×400). A similar increase in β-galactosidase expression was observed in the liver (19.92-fold) and heart (7.32-fold) of transgenic mice exposed to the adenine diet compared with transgenic mice on a normal diet (Figure 3b and c). For the aorta, the β-galactosidase signal intensity was measured specifically in the wall along a line extending from the intima to the adventitia (Supplementary Figure S4B). A 1.82-fold increase ($P = 0.0275$) in β-galactosidase expression was observed in the aortic wall of adenine-induced CKD mice. Analysis of brain tissue revealed microvessels positive for β-galactosidase (Figure 3b). Further quantitation revealed an 8-fold increase in the average number of microvessels per square millimeter positive for β-galactosidase in mice on the adenine diet (8.630 ± 1.692) compared with those on the normal diet (1.425 ± 1.145) ($P = 0.048$) (Figure 3c). A correlation analysis was performed to demonstrate the relationship between the levels of BUN or IS in the CKD model and the extent of AHR activation in the tissues of adenine-exposed mice (Table 1). We observed a strong and significant correlation between the levels of BUN or IS and β-galactosidase protein expression in the organs. This finding strengthens the relationship between AHR activation in various tissues and increased BUN (reflective of deterioration of renal function) or IS levels in the CKD model. Taken together, these results demonstrate AHR activation within specific tissues of different organs in a CKD model.

Table 1 | Correlations between β-gal expression and IS and BUN levels for organs of adenine-exposed mice

Parameter	Spearman correlation coefficient *r*	*P*
BUN and IS	0.9048	0.0046
BUN and β-gal (kidney)	0.7143	0.0491
BUN and β-gal (liver)	0.8264	0.0154
BUN and β-gal (heart)	0.7381	0.0458
BUN and β-gal (CNS)	0.8189	0.0154
IS and β-gal (kidney)	0.7619	0.0368
IS and β-gal (liver)	0.7545	0.0368
IS and β-gal (heart)	0.7381	0.0458
IS and β-gal (CNS)	0.7433	0.0480

BUN, blood urea nitrogen; β-gal, β-galactosidase; CNS, central nervous system; IS, indoxyl sulfate.

Tissue-specific activation of AHR in an IS-specific model

To examine whether IS can recapitulate the pattern of AHR activation observed with adenine-induced CKD model, we used an IS-specific model as described previously.[10] This model is characterized by an increase in IS to a level similar to that in patients with end-stage renal disease (ESRD) without alteration of renal function.[10]

AHR activation in various tissues in response to IS was confirmed by quantitative real-time polymerase chain reaction, which showed significant increases in *β-galactosidase* mRNA in the liver, kidney, and heart (Figure 4a). Our quantitative analysis of different tissues revealed a significant increase in β-galactosidase protein expression by 8.76-fold in the kidney, 14.21-fold in the liver, and 6.37-fold in the heart (Figure 4b and c). Similarly to the adenine-induced CKD model, the IS-specific model showed 26% to 30% ($P = 0.0286$) increase in β-galactosidase expression in the intima and media of the aorta of IS-treated animals compared with controls (Figure 4b and c). There was a trend toward an increased number of β-galactosidase–positive microvessels of the central nervous system in mice treated with IS compared with controls (Figure 4b, arrow, and c).

Figure 3 | Aryl hydrocarbon receptor activation in an adenine-induced chronic kidney disease model. Transgenic mice were administered a diet supplemented with 0.25% adenine for 2 weeks. Transgenic mice on a normal diet served as controls. (**a**) β-Galactosidase mRNA was examined in whole tissue lysates in transgenic mice and normalized to glyceraldehyde-3-phosphate dehydrogenase mRNA. Each data point represents the average of duplicate samples for each transgenic mouse used. (**b**) Representative frozen sections stained with anti–β-galactosidase antibody are shown. The β-galactosidase protein was localized to renal tubules (marked by a black asterisk), liver hepatocytes, and cardiac myocytes (black arrow). In addition, β-galactosidase expression was seen in microvessels of the central nervous system (CNS) (black arrowhead). (**c**) A color-based image segmentation pipeline (see the Supplementary Methods) was used to quantify the increase in β-galactosidase expression per tissue area in the kidney, liver, and heart. The number of microvessels of the CNS positive for β-galactosidase was counted and presented as the number of positive microvessels per square millimeter. All data are expressed as mean ± SEM. Images of the kidney, liver, heart, and aorta were taken at original magnification ×200. Bar = 50 μM. Images in the CNS were taken at original magnification ×400. Bar = 25 μM. L, lumen; V, vessel wall. To optimize viewing of this image, please see the online version of this article at www.kidney-international.org.

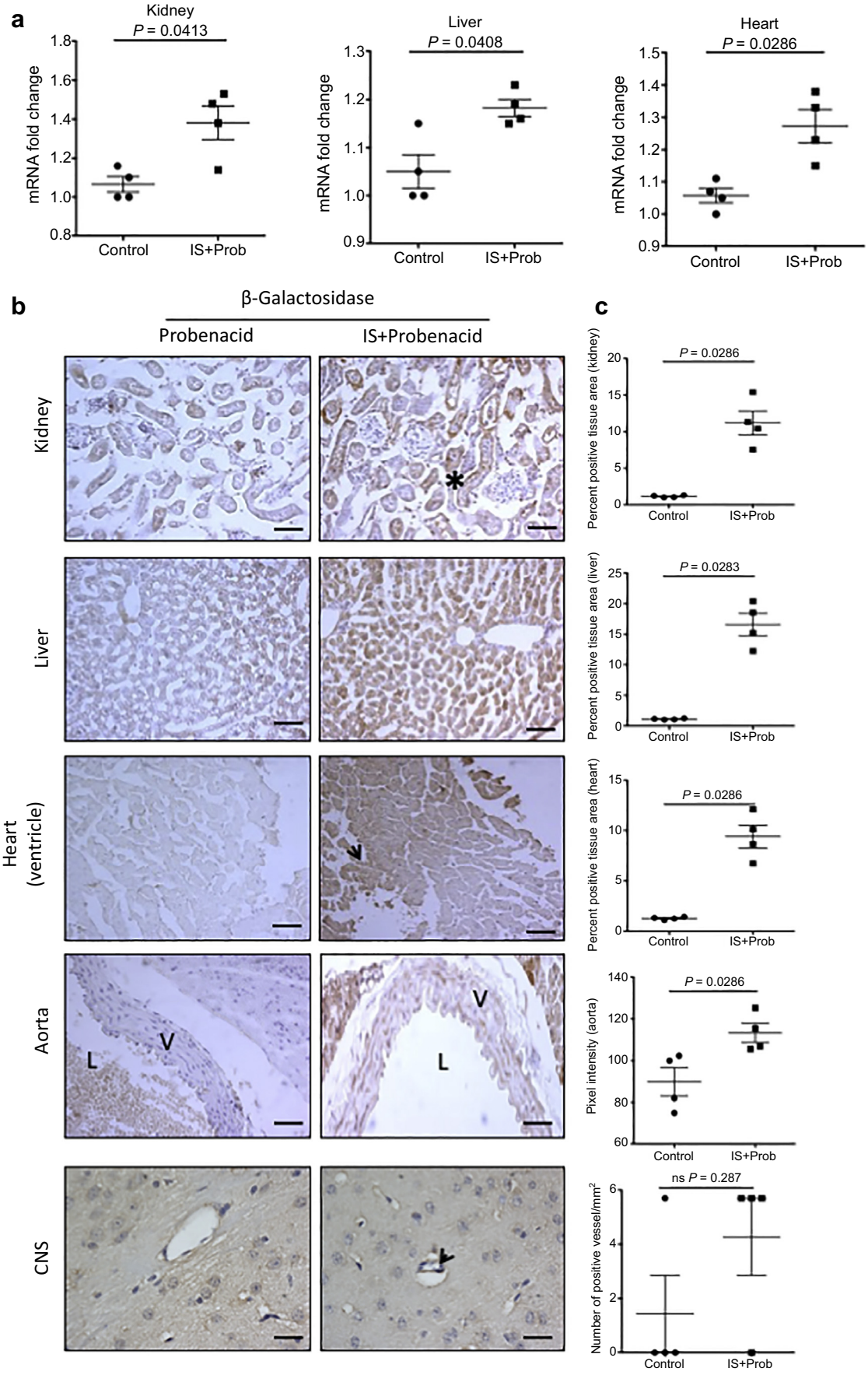
a
Kidney
P = 0.0413
mRNA fold change
Control
IS+Prob
Liver
P = 0.0408
mRNA fold change
Control
IS+Prob
Heart
P = 0.0286
mRNA fold change
Control
IS+Prob
b
β-Galactosidase
Probenacid
IS+Probenacid
Kidney
Liver
Heart (ventricle)
Aorta
CNS
V
L
c
P = 0.0286
Percent positive tissue area (kidney)
Control
IS+Prob
P = 0.0283
Percent positive tissue area (liver)
Control
IS+Prob
P = 0.0286
Percent positive tissue area (heart)
Control
IS+Prob
P = 0.0286
Pixel intensity (aorta)
Control
IS+Prob
ns P = 0.287
Number of positive vessel/mm2
Control
IS+Prob

We further probed the level of AHR activation in kidneys using cell type–specific markers for both proximal (aquaporin 1) and distal (uromodulin) tubules and endothelial cells (CD31) (Supplementary Figure S6 and Supplementary Table S2). Staining of consecutive kidney sections with β-galactosidase and the above markers showed the presence of β-galactosidase stain in the tubules positive for aquaporin 1 or uromodulin, suggesting AHR activation in both proximal and distal renal tubules. Similar to the adenine-induced CKD model, the β-galactosidase signal was not observed in the glomeruli, but rather in the periglomerular region (Supplementary Figure S5). The endothelial cells of the arterioles within the kidneys stained with CD31 were also positive for β-galactosidase, corroborating the findings in the aortas of adenine- and IS-exposed mice (Supplementary Figure S6). A similar analysis in the adenine-induced CKD model could not be performed because of the distorted tubules and extensive renal damage at the time of harvest. These results confirmed IS as an activator of the AHR pathway in various organs and could explain AHR activation observed in the adenine-induced CKD model.

Temporal activation of AHR in an I/R-induced AKI model

Because indolic solutes are also elevated in AKI in patients,[25] we examined AHR activation in an established mouse model of AKI, I/R injury. Because I/R injury models are known to have a distinct predilection for male mice,[26] this experiment was conducted in a group of male transgenic mice. I/R injury rapidly increased the BUN level at 24 and 48 hours post-surgery, and as expected, it decreased by 96 hours (Supplementary Figure S3C).

The kidneys of I/R injury mice showed a significant increase in *β-galactosidase* mRNA by 34.3% ($P = 0.0301$) and 29.0% ($P = 0.0328$) at 24 and 48 hours post–I/R injury, respectively (Figure 5a, left). Similarly, increased *β-galactosidase* mRNA was observed in the liver (Figure 5a, right). *β-Galactosidase* mRNA was significantly increased by 25.7% ($P = 0.0438$) at 24 hours postsurgery and by 27.0% ($P = 0.0435$) at 48 hours postsurgery in the kidney and liver, respectively. In contrast, no change in *β-galactosidase* mRNA was observed in the heart or central nervous system of I/R injury mice.

In the same vein, I/R injury resulted in a significant 9.91-fold ($P = 0.0079$) and 14.27-fold ($P = 0.0195$) increase in β-galactosidase protein expression in the tubules and hepatocytes, respectively, at 24 hours postsurgery (Figure 5b and e), which persisted up to 96 hours post–I/R injury (Figure 5c–e). The above-mentioned results suggest that AKI-induced AHR activation was localized in the kidney and liver and persisted despite a decrease in BUN and IS levels.

Relationship between kinetics of AHR activation and uremic solutes

Because CKD and AKI in humans are characterized by increased levels of uremic toxins,[5,27] we posited that AHR activation in tissues is likely to coincide with the increase in the levels of uremic solutes. We specifically examined IS and kynurenine in the plasma, which are known to activate AHR signaling.[8,9] Plasma IS levels increased 4.79-fold in adenine-induced mice compared with mice on a normal diet ($P = 0.0286$) (Figure 6a). A similar trend was observed with kynurenine ($P = 0.0286$) (Figure 6a). In the IS-specific model, plasma IS levels increased 18.03-fold compared with control mice (Figure 6b, right). Plasma levels of kynurenine remained similar between the 2 groups (Figure 6b). The increase in IS levels coincided with the increased β-galactosidase protein expression in various organs in both these models (Figures 2 and 3). In the I/R injury model, the levels of IS significantly increased 1.76-fold 24 hours post-surgery ($P = 0.043$) and then declined rapidly (Figure 6c). There were no differences at any time point in levels of plasma kynurenine (Figure 6c). β-Galactosidase expression persisted even with normalization of IS levels.

DISCUSSION

In this study, we demonstrated tissue-specific activation of the AHR pathway in response to discrete mouse models of kidney diseases. The choice of models was driven by the hypothesis that focuses on AHR activation by indolic uremic solutes. Among various models of CKD,[23] we used the adenine model because it is known to increase IS to a level corresponding to that in patients with end-stage renal disease.[10] The time points selected for different models were driven by the prospects of obtaining a signal for β-galactosidase given the low transgene activity in this model.[21] For example, the adenine-induced model results in persistent accumulation of uremic toxins over a 2-week period after exposure to a 0.25% adenine–supplemented diet.[28] The IS-specific model results in increased levels of IS analogous to different stages of CKD.[10] For both these models, AHR expression was examined at 2 time points. In general, AKI in humans and rodents results in compromised renal function and accumulation of indolic uremic solutes that improves with the recovery of renal function.[25]

Figure 4 | Tissue-specific expression of β-galactosidase expression in an indoxyl sulfate (IS)–specific model. (**a**) β-Galactosidase mRNA was examined in whole tissue lysates in transgenic mice and normalized to glyceraldehyde-3-phosphate dehydrogenase mRNA. (**b**) Representative frozen sections stained with anti–β-galactosidase antibody are shown from the kidney, liver, heart, and central nervous system (CNS). (**c**) A color-based image segmentation pipeline was used to quantify the increase in β-galactosidase expression per tissue area in the kidney (marked by a black asterisk), liver, and heart (black arrowhead). The number of microvessels of the CNS positive for β-galactosidase was counted and presented as the number of positive microvessels per square millimeter (black arrow). Each data point represents the average of 5 random fields of view analyzed for the percent positive tissue area for each transgenic mouse (control, n = 4; IS, n = 4). All data are expressed as mean ± SEM. Images of the kidney, liver, heart, and aorta are taken at original magnification ×200. Bar = 50 μM. Images in the CNS were taken at original magnification ×400. Bar = 25 μM. L, lumen; Prob, probenecid; V, vessel wall. To optimize viewing of this image, please see the online version of this article at www.kidney-international.org.

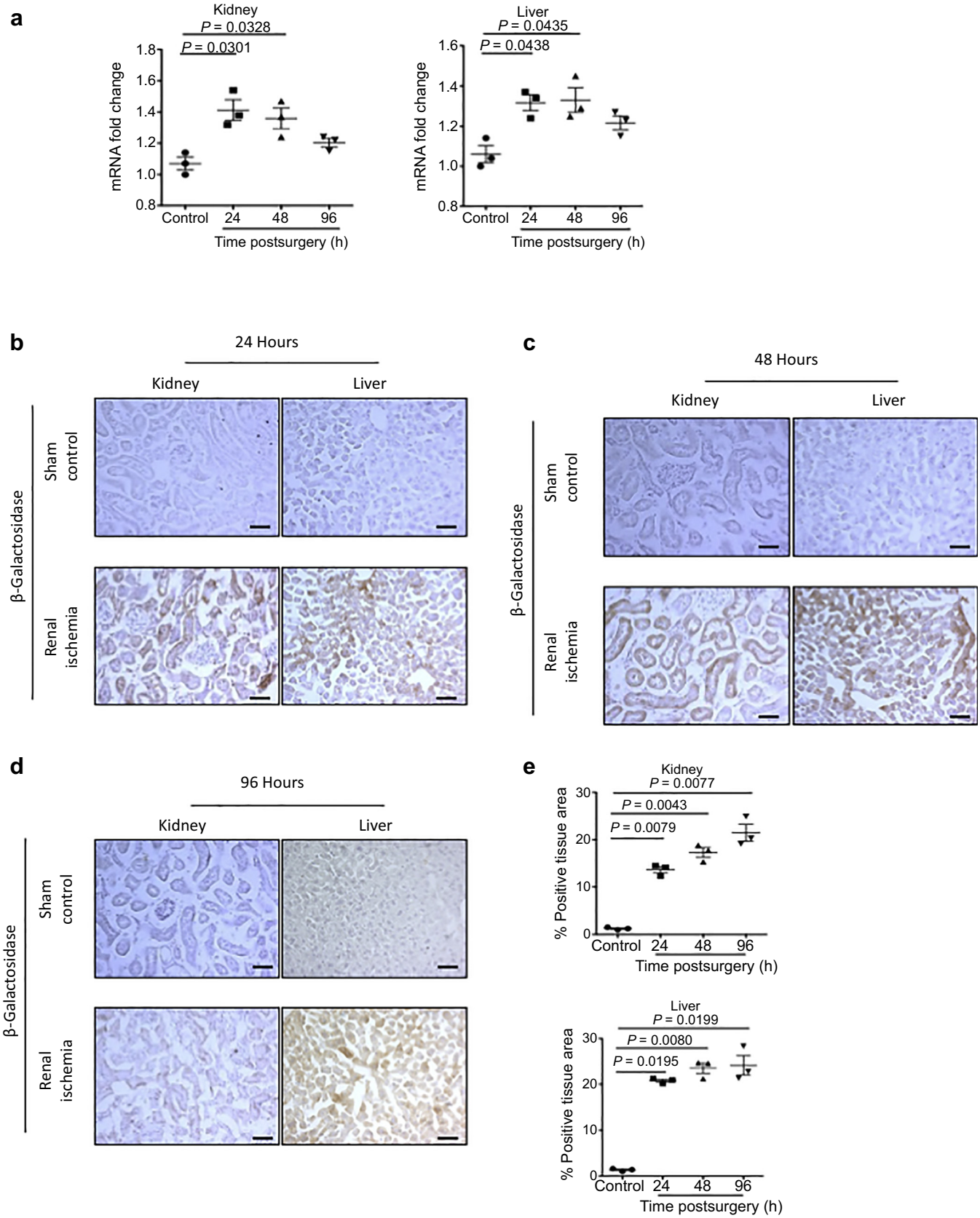

Figure 5 | Aryl hydrocarbon receptor (AHR) activation in the renal ischemia/reperfusion model of acute kidney injury. AHR activation was examined in transgenic mice after 23 minutes of bilateral renal ischemia. Groups of mice were killed at 24 (**a**), 48 (**b**), and 96 (**c**) hours postsurgery. (**a**) β-Galactosidase mRNA was examined in whole tissue lysates in transgenic mice and normalized to (continued)

Therefore, we performed the kinetic analysis of AHR activation in organs at 3 time points in the I/R injury model.

Data obtained by this investigation provide hypothesis-generating insights into uremic toxicity. Adenine and IS exposure increased AHR activity in the proximal and distal renal tubules. AHR signaling regulates fundamental cellular processes such as apoptosis, cell proliferation, and cell cycle by regulating B-cell lymphoma 2 (BCL2), Fas receptor (FasR), and cell cycle kinases.[29,30] With the renal insult, tubular cell proliferation and survival are pivotal to maintain the functional renal tubular mass. Our results showing AHR activation in renal tubules by IS warrant further studies to examine the role of AHR in progressive tubular damage.

Interestingly, adenine- and IS-exposed kidneys showed AHR activation in the periglomerular region (Supplementary Figure S5). Although it is difficult to precisely discern the cell type involved, the presence of an AHR signal in the periglomerular region is intriguing. Renal fibrosis involves different compartments such as the tubulointerstitial and periglomerular regions. AHR signaling has been implicated in the fibrosis of different organs. AHR interacts with the p65 subunit of nuclear factor-κB transcription factors and also changes the chemokine profile through an AHR–IL-22 axis, altering fibrosis in the lung in cystic fibrosis.[31–33] In fact, the aryl hydrocarbon nuclear translocator (ARNT), a transcriptional coactivator of AHR, has been implicated in renal fibrosis and sought as a therapeutic target in CKD.[34] A possible connection between AHR and renal fibrosis is further supported by the reports that link the indolic solutes to renal fibrosis,[35] which may be mediated through AHR signaling. Taken together, further studies are needed to investigate the role of AHR signaling in the kidneys, especially because AHR perturbations have different effects in various organs.

AHR signaling is the main regulator of cytochrome P450. There are >200 P450 proteins, of which AHR signaling regulates 3 members, *CYP1A1*, *CYP1A2*, and *CYP1B1*, which are the AHR ligand metabolizing P450 proteins.[36] AHR can potentially alter the pharmacokinetics of drugs metabolized specifically by the CYP1 family. Also, AHR activation can alter the pharmacokinetics of drugs through other mechanisms. For example, Santana *et al.* demonstrated that IS, through AHR activation, regulates the transporter protein such as P-glycoprotein to influence the blood levels of immunosuppressive medications.[37] The effect of AHR activation on the pharmacokinetics of drugs remains an underexplored area and is relevant given polypharmacy in patients with CKD.

Cardiovascular disease constitute a major cause of mortality in patients with CKD. The present results showing AHR activation in cardiac myocyte and vasculature have pathogenic implications. In a zebra fish model, AHR activation in cardiac myocytes exhibited a phenotype similar to congestive heart failure as well as reduced peripheral blood flow.[38] The relevance of these findings to patients with CKD is important because patients with CKD develop congestive heart failure with low ejection fraction and with preserved ejection fraction.[39] Patients with CKD are at a higher risk of atherothrombotic vascular disease. AHR activation in aorta potential has functional consequences given its known role in atherosclerosis[40,41] and that accelerated atherosclerosis is a known manifestation of uremia.[42,43] Although previous studies had demonstrated the presence of the AHR protein in the vessel wall or AHR activation in cultured endothelial and vascular smooth muscle cells, there was no direct *in vivo* evidence of cell type–specific activtion of AHR in the vasculature in response to kidney disease models. In that regard, the present work supports the previous studies[9,10,11] and provides an *in vivo* proof of AHR activation in the vessel wall in different models of CKD. It is noteworthy that AHR activation in the vessel walls is associated with increased stiffness and an aging phenotype.[44] A similar phenomenon was observed by Nath *et al.* in a mouse model of the arteriovenous fistula in the uremic milieu,[45] raising a possiblity of the influence of the AHR pathway on dialysis access malfunction.

Patients with CKD of all stages are at an increased risk of cognitive decline.[46] In patients on hemodialysis, the prevalence of cognitive impairment has been estimated at 30% to 60%, at least twice that observed in age-matched controls.[47,48] Although several factors are considered including white matter lesions, silent infarcts, and microbleeds,[46] fundamental to all these pathological manifestations is vascular injury. Our observations of AHR activation in the endothelial cells of the cerebral microvasculature in both the adenine-induced CKD model and IS-specific model opens possible areas of investigation in the fundamentals of endothelial biology in the central nervous system in the uremic milieu and AHR signaling.

AKI is considered to be a self-limiting event. However, emerging epidemiological studies showed profound long-term effects of a single episode of AKI.[49] For example, Ishani *et al.* reported that AKI was associated with a risk of end-stage renal disease that was 13 times higher than that in patients without AKI, and the risk of end-stage renal disease was 40 times higher if patients had AKI and preexisting CKD.[50] Our results in the I/R injury model showed persistent activation of AHR signaling in the renal tubules even after reduction in the levels of BUN and IS (Figures 5 and 6; Supplementary Figure S3C). There can be alternative explanations for this phenomenon, such as involvement of other uremic solutes or increase in the inflammatory cytokines

Figure 5 | (continued) glyceraldehyde-3-phosphate dehydrogenase mRNA. (**b–e**) Frozen sections of the kidney and liver were stained with anti–β-galactosidase antibody. A color-based image segmentation pipeline was used to measure the percentage of tissue area positive for the β-galactosidase protein. Each data point represents the average of 5 random fields of view analyzed for the percent positive tissue area for each transgenic mouse (n = 3 for each group; sham control; 24, 48, and 96 hours postsurgery; the left graph is for the kidney and the right graph for the liver). All data are expressed as mean ± SEM. Images are taken at original magnification ×200. Bar = 50 μM.
To optimize viewing of this image, please see the online version of this article at www.kidney-international.org.

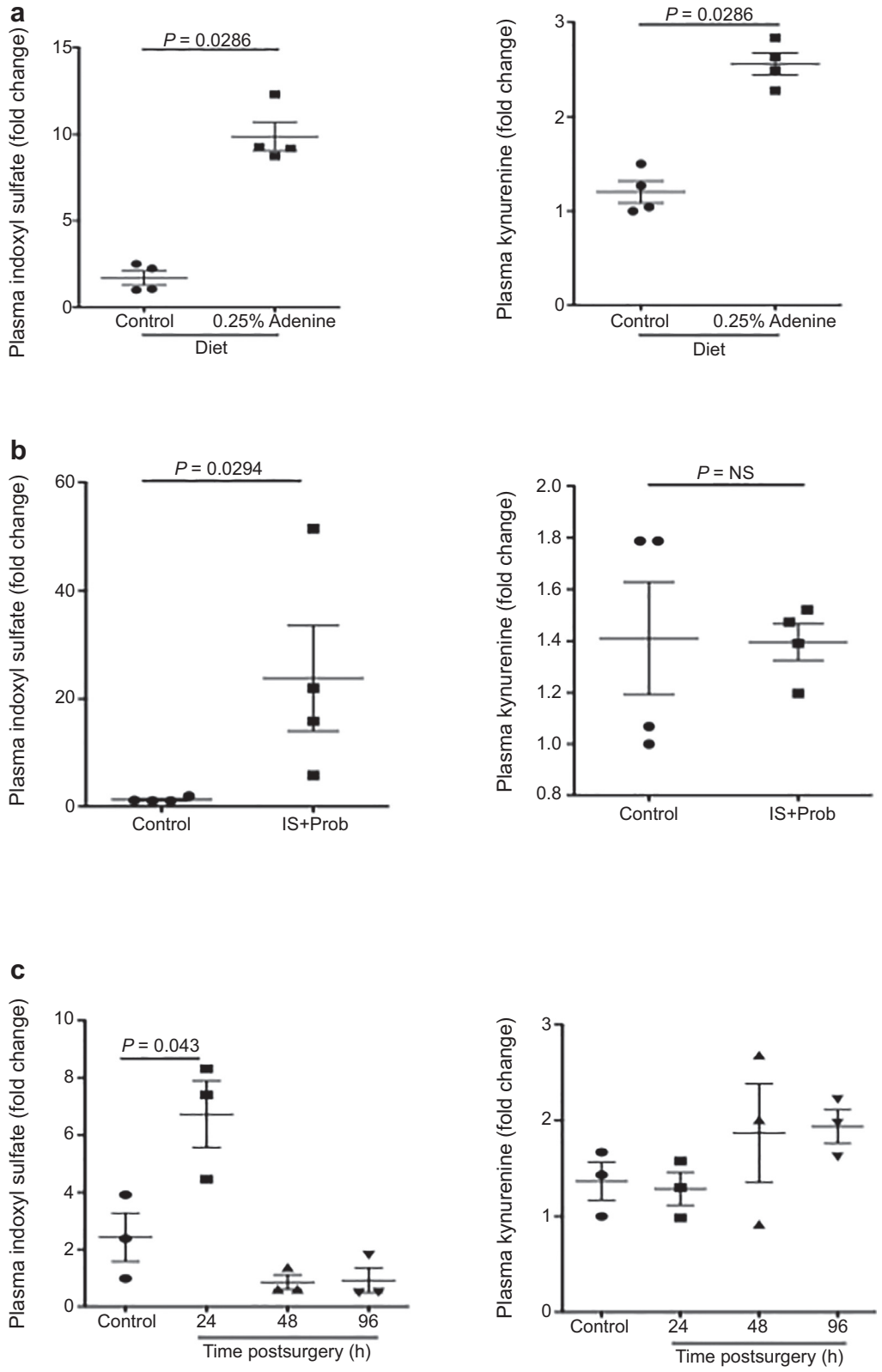

Figure 6| Concurrence between aryl hydrocarbon receptor (AHR) ligands and AHR activation in chronic kidney disease and acute kidney injury models. Uremic solutes in the plasma were determined by mass spectrometry. (**a**) Plasma samples from adenine-induced mice and controls analyzed for indoxyl sulfate (IS) and kynurenine are shown. (**b**) Plasma samples from mice receiving IS and probenecid (Prob) are shown. (**c**) Plasma from mice at different time points after ischemic/reperfusion injury was analyzed for IS and kynurenine. All data are expressed as mean ± SEM. NS, not significant.

released during AKI known to activate the AHR pathway. Irrespecitve of the mechanism, it is conceivable that persistent AHR activity may have a untoward effect on the survival of renal tubules.

A growing body of literature has shown that among different uremic solutes, tryptophan metabolites (such as IS) activate AHR signaling. Our results demonstrate AHR activation in several organs in the uremic milieu with a tissue-specific pattern, which may potentially explain some of the systemic manifestations of uremic toxicity. By illustrating the use of an *in vivo* tool, this study paves the way to systemically probe the tissue level toxicity of other uremic solutes. The results from this study warrant further mechanistic probing given that AHR signaling is a therapeutically targetable pathway.

METHODS

Animal ethics

Animals were maintained under the supervision of the Boston University animal core facility following the Institutional Animal Care and Use Committee protocol number AN-15449.2016.03. Animals were housed in conventional housing with 3 male mice per cage and 5 female mice per cage.

Overview of transgenic mouse

B6.Cg-Tg(DRE-lacZ)2Gswz/J mice (stock no. 006229) were purchased from Jackson Laboratory (Bar Harbor, ME) and housed and bred at the Boston University animal core facility. This mouse line was originally donated by Dr. Thomas A. Gasiewicz, School of Medicine and Dentistry, University of Rochester, Rochester, NY. The mouse contains a *lacZ* reporter gene downstream of 2 DREs and chicken ovalbumin TATA box as previously described.[21] Male and female transgenic mice were randomized to experimental groups for models of CKD. Male mice were used for the renal I/R injury model.

Genotyping of transgenic mice

DNA was extracted from tail clippings of all mice used in these experiments after weaning at 21 days. Mice containing the *lacZ* transgene were identified through conventional polymerase chain reaction using forward and reverse primers complementary to the transgene and an internal positive control (Table 1). After identification of mice containing the transgene, extracted genomic DNA was used as a template for quantitative real-time polymerase chain reaction to determine the copy number of the *lacZ* transgene. Genomic DNA was probed using a commercially available TaqMan probe complementary to the *lacZ* gene from Thermo Fisher Scientific (Cambridge, MA). All mice used in these experiments were homozygous for the transgene (Supplementary Figure S1).

Statistical analysis

Data were analyzed using a nonparametric Welch *t* test or analysis of variance, as indicated. Significance was accepted as $P < 0.05$. Data are expressed as mean ± SEM. Correlations between BUN levels, IS levels, and quantification of the β-galactosidase protein in all tissues were analyzed using a nonparametric Spearman correlation.

Details on administration of TCDD to B6.Cg-Tg(DRE-lacZ)2Gswz/J mice, different models of kidney diseases (adenine-induced CKD, IS-specific, and I/R injury models), tissue collection, immunohistochemistry, antibodies, image quantification, quantitative real-time polymerase chain reaction, BUN estimation, and the liquid chromatography/mass spectrometry method of determining uremic solutes are given in the Supplementary Methods.

DISCLOSURE

All the authors declared no competing interests.

ACKNOWLEDGMENTS

We thank the veterinary care staff at the Boston University animal core facility for their help in maintaining the animal colonies. We thank Boston University School of Medicine Cellular Imaging Core for their help with imaging the immunohistochemistry experimental slides. We also thank Teresa Russell (Boston University) for review of the manuscript.

This work was funded in part by NCI R01CA175382, NIH R01HL132325, and Evans Junior Faculty Merit award (VCC); NIH R01HL080442 and R01HL136363 (KR); NIEHS Superfunds Research Program grant P42ES007381 (DS); T32 training grant in cardiovascular biology T32 HL007224-40 (JAW); T32 training grant in immunobiology of trauma NIHT32GM086308-06A1 (NA); the Thrombosis to Hemostasis in Health and Disease Affinity Research Collaborative (Evans Center For Interdisciplinary Biomedical Research, Boston University); NIH/NHLBI R01HL136363 (KR); and P42ES025409 (DS).

SUPPLEMENTARY MATERIAL

Supplementary Methods.

Table S1. Primer sequences for the identification of transgenic mice.

Table S2. List of primary antibodies for immunohistochemistry.

Figure S1. Determination of copy number in B6.Cg-Tg(DRE-lacZ)2Gswz/J transgenic mice. All mice were genotyped through conventional PCR with the indicated primers. Genomic DNA from hemizygous mice was then used as a template for qRT-PCR using a commercially available TaqMan probe complementary to the *lacZ* (green) gene to determine the copy number. Data were normalized to GAPDH (red). A representative Ct graph of 3 independent experiments is shown.

Figure S2. Dre-LacZ transgenic mice were administered TCDD and killed after 4 days. Untreated transgenic mice served as controls. Fresh liver tissue was harvested, and consecutive slides were stained with a β-galactosidase reporter gene staining kit (Sigma, catalogue number GALS-1LT) and prevalidated anti–β-galactosidase antibody (**A**). Consecutive sections of the liver from the same were stained with prevalidated anti–β-galactosidase antibody and isotype control to show specificity of the antibody used for immunohistochemistry (IHC). Mice showed prominent stain for the β-galactosidase protein using IHC (**B**). Representative images of liver tissue at 200× magnification are shown.

Figure S3. Blood urea nitrogen determination. Renal function was assessed on the terminal plasma from all mice by measuring blood-urea nitrogen (BUN. BUN was determined following the manufacturer's protocol by using a QuantiChrom Urea Assay Kit (DIUR-100) from Bioassay Systems. In mice exposed to a 0.25% adenine–supplemented diet, there was an ∼4-fold increase in BUN levels compared with controls (**A**). In the IS-specific model of CKD, BUN was not increased between mice treated with IS and control mice (**B**). In the renal ischemia/reperfusion model of acute kidney injury (AKI), BUN increased significantly at 24 hours postsurgery and remained elevated at 48 hours while decreasing at 96 hours postsurgery (**C**).

Figure S4. Image quantification of β-galactosidase protein expression. A customized, color-based image segmentation pipeline was used to quantify the amount of β-galactosidase and expressed as percent positive tissue area for the kidney, liver, and heart in tissue from animal models of CKD and AKI. Briefly, RGB color images were converted to L*a*b* color space with the 2-dimensional a*b* space

data used for further analysis, with each image segmented into 3 clusters and the percentage of tissue area positive for β-galactosidase analyzed (**A**). For the aorta, the amount of the β-galactosidase protein was analyzed by measuring the pixel intensity of a gray scale image along a line from the intima to the adventitia. Five lines were measured per section of the aorta (**B**).

Figure S5. β-Galactosidase protein expression in the periglomerular space. Kidneys from both the adenine-induced model of CKD and the IS-solute–specific model of uremia were stained with an antibody against β-galactosidase. High magnification imaging (400×) shows AHR activation, indicative of β-galactosidase expression, in the periglomerular fibrotic regions. For 200× magnification images, bar = 50 μM. For 400× magnification images, bar = 25 μM.

Figure S6. Tissue-specific AHR activation in a solute-specific model of CKD. To examine tissue-specific localization of AHR in an IS-specific model of CKD, serial sections from transgenic mice that received IS with probenecid for 4 days were stained with antibodies against β-galactosidase (AHR acitvation) and one of the following: uromodulin (distal tubules), aquaporin 1 (proximal tubules), and CD31 (endothelial cells). (**A**) β-Galactosidase was found to be expressed in distal tubules marked by expression of uromodulin. (**B**) In addition, proximal tubules marked by expression of aquaporin 1 were found to express β-galactosidase. (**C**) Kidney sections were stained with antibody against CD31, a marker of endothelial cells. We found expression of β-galactosidase in the wall of vessels in the kidney marked by expression of CD31.

Supplementary material is linked to the online version of the paper at www.kidney-international.org.

REFERENCES

1. Bowe B, Xie Y, Li T, et al. Changes in the US burden of chronic kidney disease from 2002 to 2016: an analysis of the global burden of disease study. *JAMA Network Open*. 2018;1:e184412.
2. Sirich TL. Obstacles to reducing plasma levels of uremic solutes by hemodialysis. *Semin Dial*. 2017;30:403–408.
3. Vanholder R, Glorieux G. Introduction: uremic toxicity—state of the art 2014. *Semin Nephrol*. 2014;34:85–86.
4. Vanholder R, De Smet R, Lameire N. Protein-bound uremic solutes: the forgotten toxins. *Kidney Int Suppl*. 2001;78:S266–S270.
5. Duranton F, Cohen G, De Smet R, et al. Normal and pathologic concentrations of uremic toxins. *J Am Soc Nephrol*. 2012;23:1258–1270.
6. Dou L, Jourde-Chiche N, Faure V, et al. The uremic solute indoxyl sulfate induces oxidative stress in endothelial cells. *J Thromb Haemost*. 2007;5:1302–1308.
7. Ying Y, Yang K, Liu Y, et al. A uremic solute, *p*-cresol, inhibits the proliferation of endothelial progenitor cells via the p38 pathway. *Circ J*. 2011;75:2252–2259.
8. Kolachalama VB, Shashar M, Alousi F, et al. Uremic solute-aryl hydrocarbon receptor-tissue factor axis associates with thrombosis after vascular injury in humans. *J Am Soc Nephrol*. 2018;29:1063–1072.
9. Shivanna S, Kolandaivelu K, Shashar M, et al. The aryl hydrocarbon receptor is a critical regulator of tissue factor stability and an antithrombotic target in uremia. *J Am Soc Nephrol*. 2016;27:189–201.
10. Shashar M, Belghasem ME, Matsuura S, et al. Targeting STUB1-tissue factor axis normalizes hyperthrombotic uremic phenotype without increasing bleeding risk. *Sci Transl Med*. 2017;9(417).
11. Gondouin B, Cerini C, Dou L, et al. Indolic uremic solutes increase tissue factor production in endothelial cells by the aryl hydrocarbon receptor pathway. *Kidney Int*. 2013;84:733–744.
12. Lekawanvijit S, Adrahtas A, Kelly DJ, et al. Does indoxyl sulfate, a uraemic toxin, have direct effects on cardiac fibroblasts and myocytes? *Eur Heart J*. 2010;31:1771–1779.
13. Yisireyili M, Shimizu H, Saito S, et al. Indoxyl sulfate promotes cardiac fibrosis with enhanced oxidative stress in hypertensive rats. *Life Sci*. 2013;92:1180–1185.
14. Adesso S, Magnus T, Cuzzocrea S, et al. Indoxyl sulfate affects glial function increasing oxidative stress and neuroinflammation in chronic kidney disease: interaction between astrocytes and microglia. *Front Pharmacol*. 2017;8:370.
15. Henry EC, Welle SL, Gasiewicz TA. TCDD and a putative endogenous AhR ligand, ITE, elicit the same immediate changes in gene expression in mouse lung fibroblasts. *Toxicol Sci*. 2010;114:90–100.
16. Tanaka H, Sirich TL, Meyer TW. Uremic solutes produced by colon microbes. *Blood Purif*. 2015;40:306–311.
17. Velasquez MT, Centron P, Barrows I, et al. Gut microbiota and cardiovascular uremic toxicities. *Toxins (Basel)*. 2018;10(7).
18. Mehrabi MR, Steiner GE, Dellinger C, et al. The arylhydrocarbon receptor (AhR), but not the AhR-nuclear translocator (ARNT), is increased in hearts of patients with cardiomyopathy. *Virchows Arch*. 2002;441:481–489.
19. Vasquez A, Atallah-Yunes N, Smith FC, et al. A role for the aryl hydrocarbon receptor in cardiac physiology and function as demonstrated by AhR knockout mice. *Cardiovasc Toxicol*. 2003;3:153–163.
20. Juricek L, Coumoul X. The aryl hydrocarbon receptor and the nervous system. *Int J Mol Sci*. 2018;19(9).
21. Willey JJ, Stripp BR, Baggs RB, Gasiewicz TA. Aryl hydrocarbon receptor activation in genital tubercle, palate, and other embryonic tissues in 2,3,7,8-tetrachlorodibenzo-*p*-dioxin-responsive lacZ mice. *Toxicol Appl Pharmacol*. 1998;151:33–44.
22. Wang Y, Xie T, Zhang D, Leung PS. GPR120 protects lipotoxicity-induced pancreatic β-cell dysfunction through regulation of PDX1 expression and inhibition of islet inflammation. *Clin Sci (Lond)*. 2019;133:101–116.
23. Lim BJ, Yang HC, Fogo AB. Animal models of regression/progression of kidney disease. *Drug Discov Today Dis Models*. 2014;11:45–51.
24. Shashar M, Siwak J, Tapan U, et al. c-Cbl mediates the degradation of tumorigenic nuclear β-catenin contributing to the heterogeneity in Wnt activity in colorectal tumors. *Oncotarget*. 2016;7:71136–71150.
25. Wang W, Hao G, Pan Y, et al. Serum indoxyl sulfate is associated with mortality in hospital-acquired acute kidney injury: a prospective cohort study. *BMC Nephrol*. 2019;20:57.
26. Wei Q, Dong Z. Mouse model of ischemic acute kidney injury: technical notes and tricks. *Am J Physiol Renal Physiol*. 2012;303:F1487–F1494.
27. Herget-Rosenthal S, Glorieux G, Jankowski J, Jankowski V. Uremic toxins in acute kidney injury. *Semin Dial*. 2009;22:445–448.
28. Jia T, Olauson H, Lindberg K, et al. A novel model of adenine-induced tubulointerstitial nephropathy in mice. *BMC Nephrol*. 2013;14:116.
29. Zaher H, Fernandez-Salguero PM, Letterio J, et al. The involvement of aryl hydrocarbon receptor in the activation of transforming growth factor-beta and apoptosis. *Mol Pharmacol*. 1998;54:313–321.
30. Mohammadi S, Seyedhosseini FS, Behnampour N, Yazdani Y. Indole-3-carbinol induces G1 cell cycle arrest and apoptosis through aryl hydrocarbon receptor in THP-1 monocytic cell line. *J Recept Signal Transduct Res*. 2017;37:506–514.
31. Beamer CA, Shepherd DM. Role of the aryl hydrocarbon receptor (AhR) in lung inflammation. *Semin Immunopathol*. 2013;35:693–704.
32. Puccetti M, Paolicelli G, Oikonomou V, et al. Towards targeting the aryl hydrocarbon receptor in cystic fibrosis. *Mediators Inflamm*. 2018;2018:1601486.
33. Weidenbusch M, Rodler S, Song S, et al. Gene expression profiling of the Notch-AhR-IL22 axis at homeostasis and in response to tissue injury. *Biosci Rep*. 2017;37(6).
34. Haase VH. ARNT as a novel antifibrotic target in CKD. *Am J Kidney Dis*. 2019;73:281–284.
35. Mutsaers HA, Stribos EG, Glorieux G, et al. Chronic kidney disease and fibrosis: the role of uremic retention solutes. *Front Med (Lausanne)*. 2015;2:60.
36. Fujii-Kuriyama Y, Mimura J. Molecular mechanisms of AhR functions in the regulation of cytochrome P450 genes. *Biochem Biophys Res Commun*. 2005;338:311–317.
37. Santana Machado T, Poitevin S, Paul P, et al. Indoxyl sulfate upregulates liver P-glycoprotein expression and activity through aryl hydrocarbon receptor signaling. *J Am Soc Nephrol*. 2018;29:906–918.
38. Lanham KA, Plavicki J, Peterson RE, Heideman W. Cardiac myocyte-specific AHR activation phenocopies TCDD-induced toxicity in zebrafish. *Toxicol Sci*. 2014;141:141–154.
39. Segall L, Nistor I, Covic A. Heart failure in patients with chronic kidney disease: a systematic integrative review. *Biomed Res Int*. 2014;2014:937398.
40. Sherr DH. Another important biological function for the aryl hydrocarbon receptor. *Arterioscler Thromb Vasc Biol*. 2011;31:1247–1248.
41. Wu D, Nishimura N, Kuo V, et al. Activation of aryl hydrocarbon receptor induces vascular inflammation and promotes atherosclerosis in

apolipoprotein E−/− mice. *Arterioscler Thromb Vasc Biol*. 2011;31:1260–1267.
42. Vanholder R, Schepers E, Pletinck A, et al. The uremic toxicity of indoxyl sulfate and *p*-cresyl sulfate: a systematic review. *J Am Soc Nephrol*. 2014;25:1897–1907.
43. Massy ZA, Ivanovski O, Nguyen-Khoa T, et al. Uremia accelerates both atherosclerosis and arterial calcification in apolipoprotein E knockout mice. *J Am Soc Nephrol*. 2005;16:109–116.
44. Eckers A, Jakob S, Heiss C, et al. The aryl hydrocarbon receptor promotes aging phenotypes across species. *Sci Rep*. 2016;6:19618.
45. Nath KA, O'Brien DR, Croatt AJ, et al. The murine dialysis fistula model exhibits a senescence phenotype: pathobiological mechanisms and therapeutic potential. *Am J Physiol Renal Physiol*. 2018;315:F1493–F1499.
46. Bugnicourt JM, Godefroy O, Chillon JM, et al. Cognitive disorders and dementia in CKD: the neglected kidney-brain axis. *J Am Soc Nephrol*. 2013;24:353–363.
47. Fazekas G, Fazekas F, Schmidt R, et al. Brain MRI findings and cognitive impairment in patients undergoing chronic hemodialysis treatment. *J Neurol Sci*. 1995;134:83–88.
48. Graham JE, Rockwood K, Beattie BL, et al. Prevalence and severity of cognitive impairment with and without dementia in an elderly population. *Lancet*. 1997;349:1793–1796.
49. Chawla LS, Eggers PW, Star RA, Kimmel PL. Acute kidney injury and chronic kidney disease as interconnected syndromes. *N Engl J Med*. 2014;371:58–66.
50. Ishani A, Xue JL, Himmelfarb J, et al. Acute kidney injury increases risk of ESRD among elderly. *J Am Soc Nephrol*. 2009;20:223–238.

Supplementary Figure 1

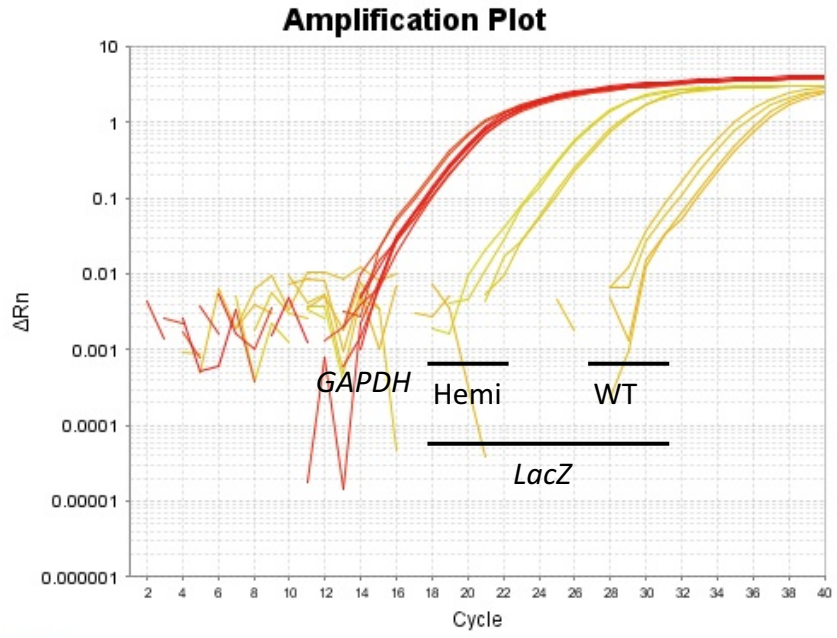

A

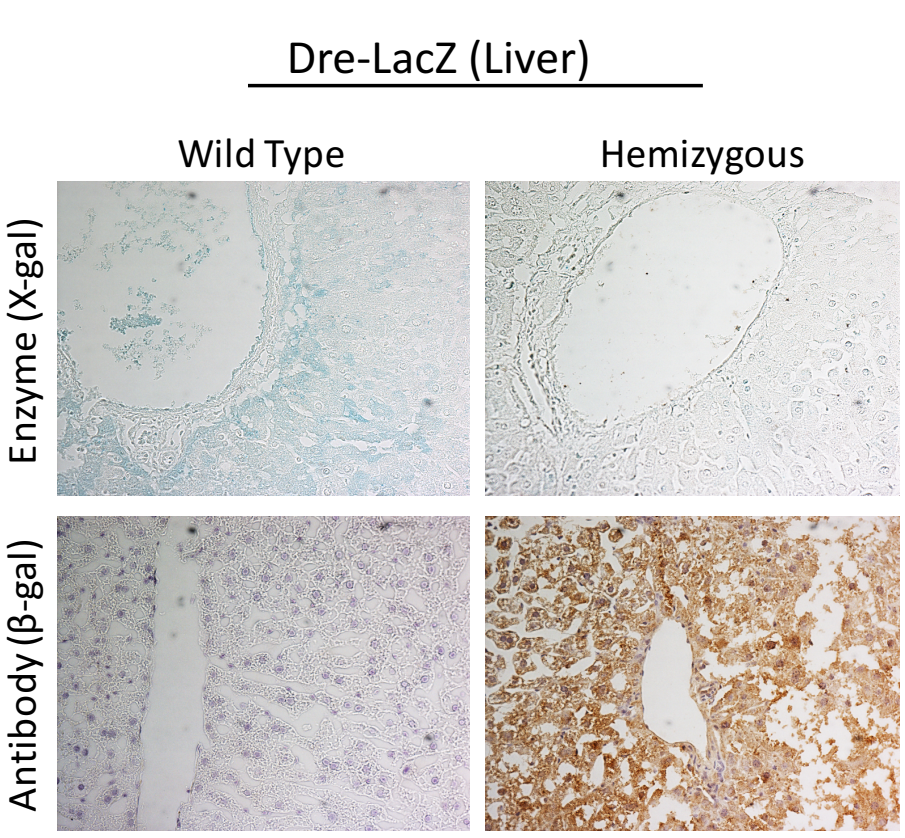
Dre-LacZ (Liver)
Wild Type
Hemizygous
Enzyme (X-gal)
Antibody (β-gal)

B

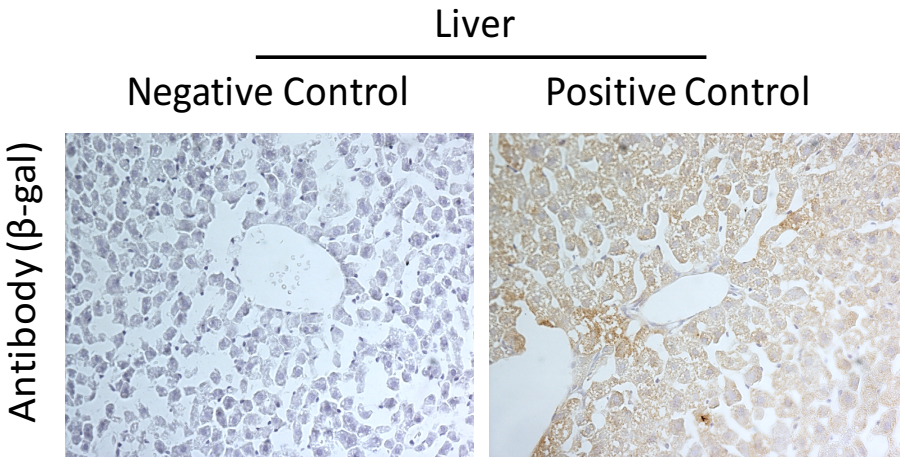
Liver
Negative Control
Positive Control
Antibody (β-gal)

A

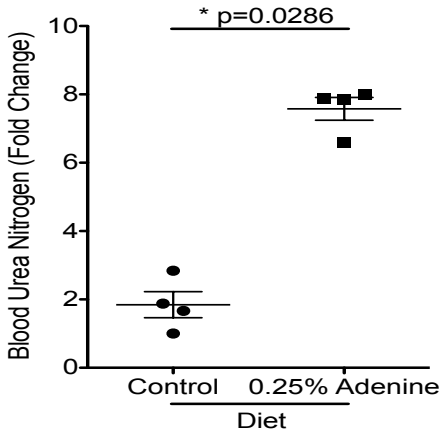
* p=0.0286
Blood Urea Nitrogen (Fold Change)
10
8
6
4
2
0
Control
0.25% Adenine
Diet

B

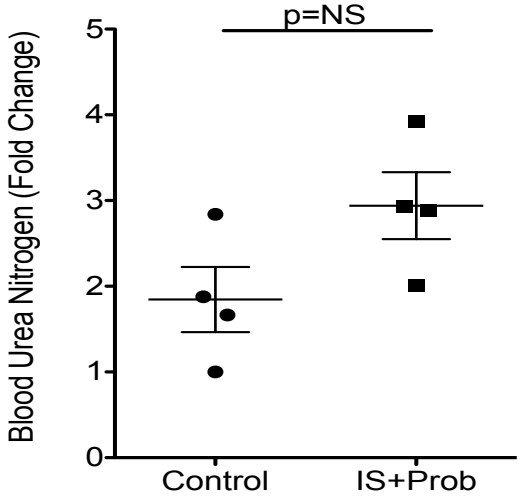
p=NS
Blood Urea Nitrogen (Fold Change)
5
4
3
2
1
0
Control
IS+Prob

C

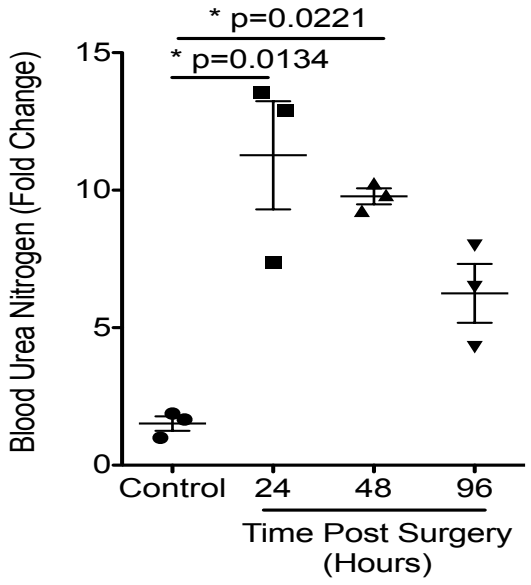
* p=0.0221
* p=0.0134
Blood Urea Nitrogen (Fold Change)
15
10
5
0
Control
24
48
96
Time Post Surgery
(Hours)

Supplementary Figure 4

A

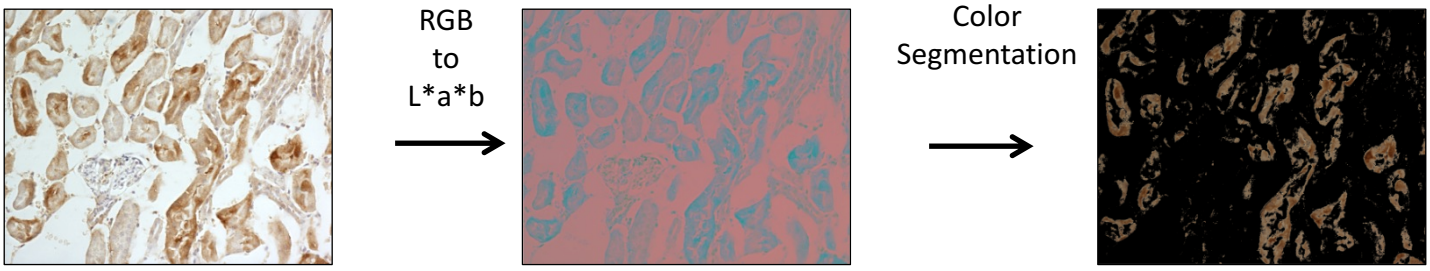

B

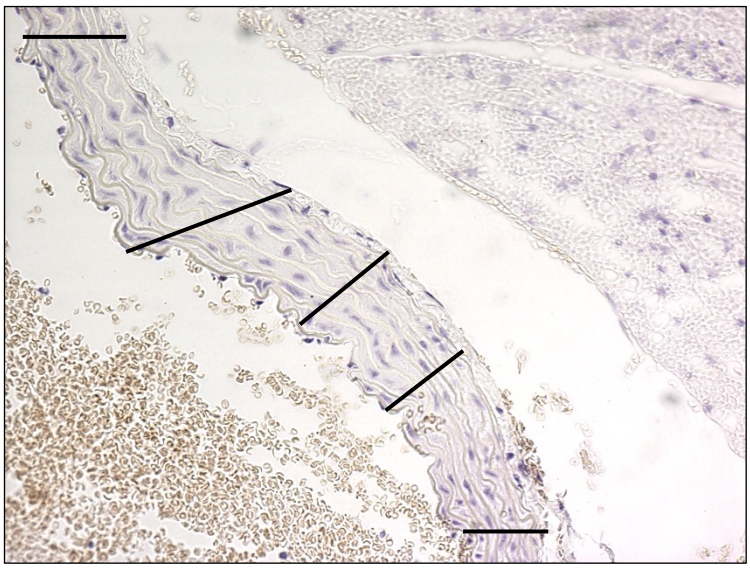

Supplementary Figure 5

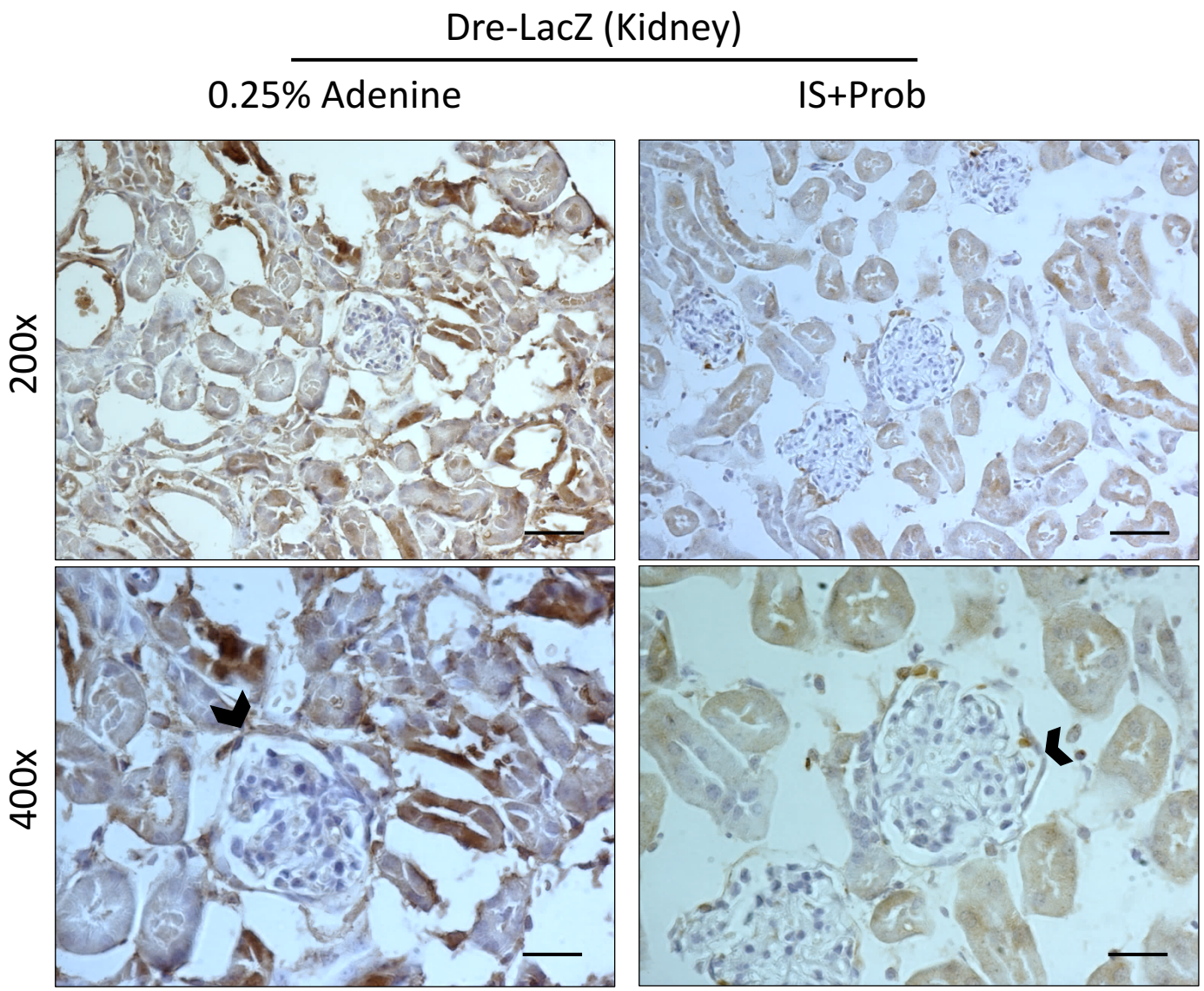

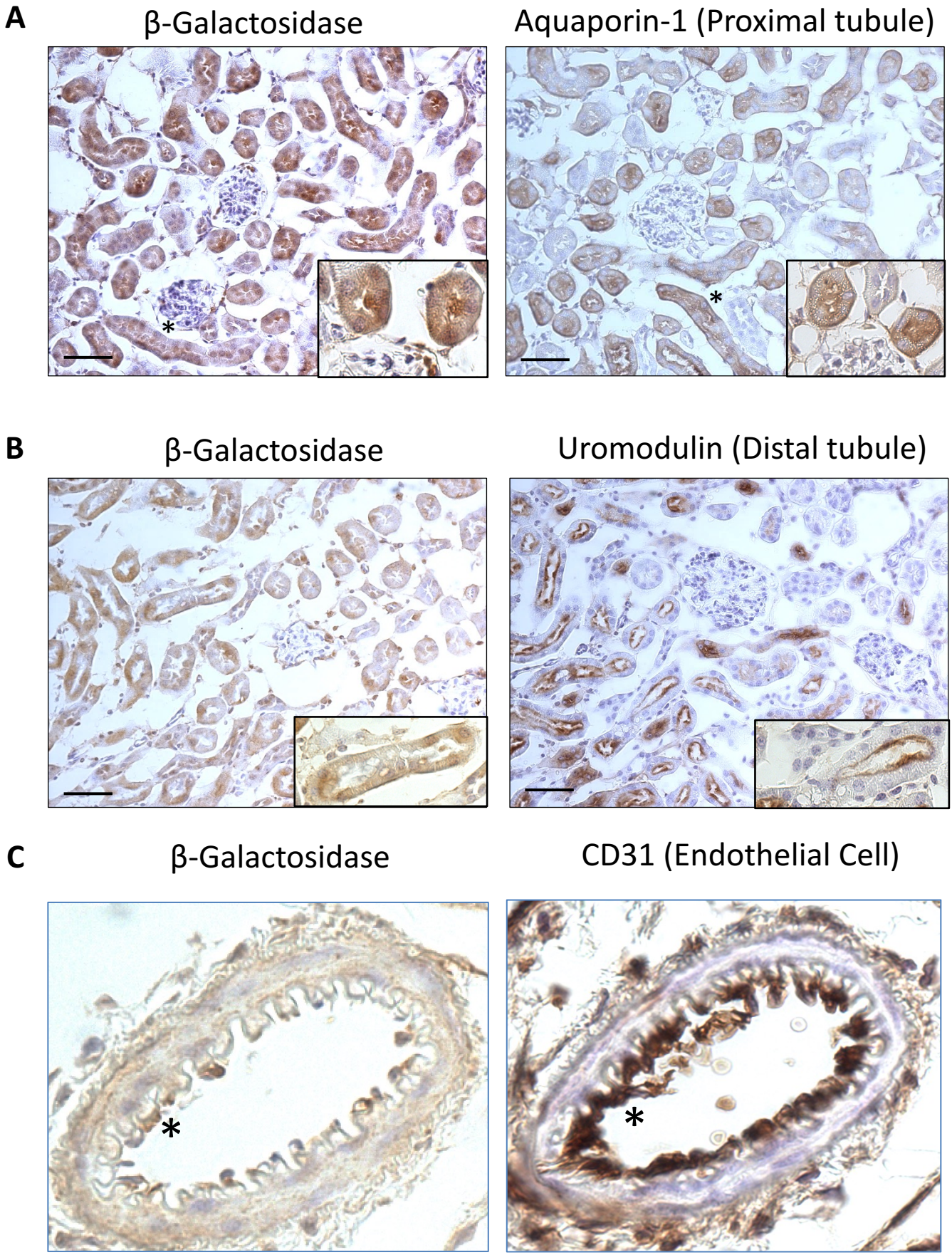
A
β-Galactosidase
Aquaporin-1 (Proximal tubule)
B
β-Galactosidase
Uromodulin (Distal tubule)
C
β-Galactosidase
CD31 (Endothelial Cell)

Supplementary Methods

Administration of TCDD to B6.Cg-Tg(DRE-lacZ)2Gswz/J:

2,3,7,8-Tetrachlorodibenzodioxin (TCDD) (kindly provided by Dr. David Sherr), a known ligand of the Aryl Hydrocarbon Receptor (AHR), was administered to 10-14 week old B6.Cg-Tg(DRE-lacZ)2Gswz/J (DRE-lacz) mice[S1] (Figure 1). Animals (n=4) were administered a single dose of 25 μg/kg TCDD, solubilized in vegetable oil, through intraperitoneal (IP) injection and kept under isolation. Four transgenic mice that received vehicle only served controls. TCDD treated DRE-lacZ mice served as positive controls for β-galactosidase (β-gal) expression in these transgenic mice (Figure 1).

Model of Kidney Disease:

Adenine Induced Chronic Kidney Disease

DRE-lacZ mice were subjected to an adenine-induced model of chronic kidney disease to evaluate tissue specific AHR activation. A group 10-14 week old male and female mice (n=4) were fed a normal diet (Teklad Global 18% Protein Rodent Diet, Envigo) supplemented with 0.25% adenine (Research Diets) for 14 days, as previously described[10]. Transgenic animals on a normal mouse diet served as controls (n=4) (Figure 1).

IS-specific animal model

A group of male and female 10-14 week-old Dre-lacZ mice (n=4) were administered indoxyl sulfate (IS) at a concentration of 4mg/mL through drinking water, ad libitum. IS excretion through OAT1

and OAT3 channels was inhibited by twice daily administration of probenecid (15 mg/kg, IP), as previously described (Figure 1)[9,10].

Renal Ischemia Reperfusion-injury model

10-14 week old DRE-lacZ male mice underwent renal ischemia reperfusion[S2]. Male mice were used for this experiment due to their increased susceptibility to renal injury following ischemia reperfusion[S3,S4]. Briefly, mice were anesthetized with isoflurane with an abdominal incision made, under sterile conditions, to access the peritoneal cavity. The renal pedicles were exposed and clamped using microvascular clamps for 23 minutes. Following the 23 minutes, the clamps were removed. A sham surgery served as control. Mouse groups were sacrificed at 24, 48, and 96 hours post-surgery (Figure 1).

Tissue Collection and Processing:

Mice were anesthetized with isoflurane and blood was collected from the carotid artery into heparin coated tubes. Plasma was separated from whole blood by centrifugation for 15min at 2000 rpm and snap frozen on liquid nitrogen. Following cervical dislocation, mice were perfused with excess 1x cold PBS. Fresh tissue was isolated from each mouse with half snap frozen on liquid nitrogen and stored at -80^{o}C for RNA extraction. The remaining tissue was cryopreserved in increasing concentrations of sucrose (15% and 30% in sterile PBS) before mounting in Optimal Cutting Temperature (OCT) mounting media. Tissue blocks were subsequently stored at -80^{o}C before sectioning.

Immunohistochemistry Image Quantification:

Frozen sections were cut using a Microm HM 550 cryostat (Thermofisher) at 5 μM. Sections were stained using the EXPOSE Mouse and Rabbit Specific HRP/DAB Detection IHC Kit (Abcam, ab80436). Briefly, frozen sections were brought to room temperature for 20 minutes before fixation in ice cold acetone for 10 minutes. Sections were washed 3x in 1x PBS for 5 minutes following by incubation in Tris-based saline with 0.05% tween (TBS-T). Endogenous peroxidase was blocked using hydrogen peroxide block for 5 minutes. Sections were washed twice in TBS-T for 5 minutes followed by incubation with serum free protein block for 15 minutes. All primary antibodies (1:1000) were incubated overnight at 4^{o}C (Supplementary table 2). Sections were washed 2x in TBS-T followed by incubation with an appropriate horseradish peroxidase (HRP) conjugate (1:500) secondary antibody for 30 minutes. The color reaction product was developed using 3,3'-diaminobenzidine tetrahydrochloride (DAB) and monitored under a microscope. Sections were counterstained in hematoxylin and dehydrated in increasing concentrations of ethanol, cleared in xylene, and mounted (Vectamount, Vector Labs). Sections were imaged using a Nikon TE-2000 wide-field microscope system. β-galactosidase expression was analyzed in tissues using a color based image segmentation pipeline previously developed[24]. For each tissue section, 5 random, 200x magnification, fields of view were imaged and analyzed. Data points are represented as the average of all fields of view for each mouse. A customized, color-based image segmentation pipeline was used to estimate the amount of β-galactosidase expression in IHC stained tissue sections, as previously described (Supplementary Figure 4A)[24]. β-galactosidase expression was analyzed by measuring the pixel intensity of a grey scale image along a line from the intima to the adventitia, in order to limit the confounding results of background stain due to connective tissue and blood cells. 5 lines were measured per section of the aorta (Supplementary Figure 4B).

Quantitative Real-Time PCR:

RNA was extracted from frozen tissue sections using the RNAeasy kit (Qiagen, cat no. 74104). cDNA was synthesized using a high-capacity cDNA reverse transcription kit (Applied Biosystems, cat no. 4368813). Quantitative real time PCR was used to detect mRNA levels in all tissue samples for β-galactosidase using Taqman probes (Thermofisher) and analyzed using a 7500 Fast Real-Time PCR System (Applied Biosystems). β-galactosidase mRNA was standardized to GAPDH mRNA for all samples. All tissue samples were analyzed in duplicate with the average ΔΔCt mean and subsequent fold change in expression determined

Measurements of Renal Function:

Renal function was assessed on terminal plasma from all mice by measuring blood-urea nitrogen (BUN). BUN was determined followed manufacturer's protocol using a Quantichrom Urea Assay Kit (DIUR-100) from Bioassay Systems. Absorbance was measured using a μQuant 96-well plate reader (Bio-Tek Instruments, Inc). Samples were analyzed in duplicate with the average BUN determined.

Measurements of Uremic Solutes: The LC/MS was conducted at the Chemistry Instrumentation Core (CIC) of Boston University.

Metabolite Extraction Procedure

Liquid chromatography/Mass spectrometry (LC/MS) was used based on a technique described previously[S5]. Serum (40 μL) was mixed with (8:1:1 Acetonitrile: Methanol: Acetone) at a 1:8 (sample: solvent) ratio, vortexed and kept on ice for 30 minutes to further precipitate proteins and lipids.

Samples were then centrifuged at 15,000 rcf for 10 minutes at <10°C to pellet proteins and lipids. Supernatant was transferred to a new, labeled tube making sure to leave behind protein pellet. Sample was dried in a speed vacuum centrifuge and then reconstituted by adding 40µl µL H_20 with 0.1% formic acid and vortexed. Samples were placed on ice for 10-15 minutes, and centrifuged to remove any protein or lipid that was not removed previously. Supernatant was transferred to a labeled glass LC vial with glass insert and placed into an Agilent HPLC 1100 series auto sampler.

LC-MS/MS

An Agilent HPLC 1100 series was used with a Waters Acquity CSH™ Phenyl-Hexyl 1.7µM 2.1 x 50mm column. For negative polarity detection of IS and IA a gradient of 95% H2O and 0.1% formic acid (buffer A) and 5% methanol (buffer B) at 0-0.5min, 95% buffer B at 5min, 98% buffer B at 8.5min, and 5% buffer B at 9.0- 10.0min at a flow rate of 0.15ml/min. A LTQ XL (Thermo Scientific) with an ESI source was used in negative mode with first event a full MS scan at 55.0-250.0m/z, isolation width 1.0, mass range normal, scan rate normal and data type profile. Scan event two was set to fragment indoxyl sulfate parent ion 212.0, CID activation with normalized collision energy 50.0, isolation width 3.0, activation Q at 0.25 and activation time of 30.0 ms. For positive polarity detection a gradient of 95% buffer A at 0.00-1.00min, 15% buffer B at 4.00min, 95% buffer B at 7.00-8.00 min, and 5% buffer B at 8.50-10.0min. In positive polarity mode the first full MS scan was at 55.0-500.0 m/z, isolation width 1.0, mass range normal, scan rate normal and data type profile. Scan event two was set to target kynurenine parent ion 209.00 m/z with a scan range of 55.0-225.0 m/z, CID activation with normalized collision energy 50.0, isolation width 3.0, activation Q at 0.25 and activation time of 30.0 ms. Wideband activation was checked.